

# ADVANCED MATERIALS

## Supporting Information

for *Adv. Mater.*, DOI: 10.1002/adma.202102421

### Precipitation Hardening in Ferroelectric Ceramics

*Changhao Zhao, Shuang Gao, Tiannan Yang, Michael Scherer, Jan Schultheiß, Dennis Meier, Xiaoli Tan, Hans-Joachim Kleebe, Long-Qing Chen, Jurij Koruza,\* and Jürgen Rödel\**

## Supplemental Information

### Precipitation hardening in ferroelectric ceramics

*Changhao Zhao, Shuang Gao, Tiannan Yang, Michael Scherer, Jan Schultheiß, Dennis Meier, Xiaoli Tan, Hans-Joachim Kleebe, Long-Qing Chen, Jurij Koruza\*, and Jürgen Rödel\**

Dr. C. Zhao, Dr. S. Gao, M. Scherer, Prof. H.-J. Kleebe, Dr. J. Koruza, Prof. J. Rödel  
Department of Materials and Earth Sciences, Nonmetallic Inorganic Materials  
Technical University of Darmstadt  
Alarich-Weiss-Straße 2, 64287 Darmstadt, Germany  
Email: [koruza@ceramics.tu-darmstadt.de](mailto:koruza@ceramics.tu-darmstadt.de)  
Email: [roedel@ceramics.tu-darmstadt.de](mailto:roedel@ceramics.tu-darmstadt.de)

Dr. J. Schultheiß, Prof. D. Meier  
Department of Materials Science and Engineering  
Norwegian University of Science and Technology  
7034 Trondheim, Norway

Dr. T. Yang, Prof. L.-Q. Chen  
Materials Research Institute and Department of Materials Science and Engineering  
The Pennsylvania State University  
University Park, Pennsylvania 16802, USA

Prof. X. Tan  
Department of Materials Science and Engineering  
Iowa State University  
Ames, Iowa 50011, USA

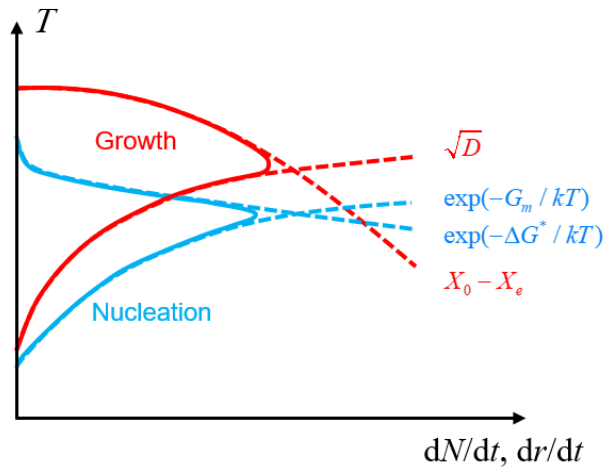


Figure S1. Temperature dependence of the precipitate nucleation rate (blue;  $dN/dt$ ) and the growth rate (red;  $dr/dt$ ).  $D$  represents the atomic interdiffusion coefficient;  $X_0$  and  $X_e$  represent the solute concentration in the matrix and at equilibrium state, respectively;  $G_m$  represents activation energy for atomic migration;  $\Delta G^*$  is the nucleation energy barrier.

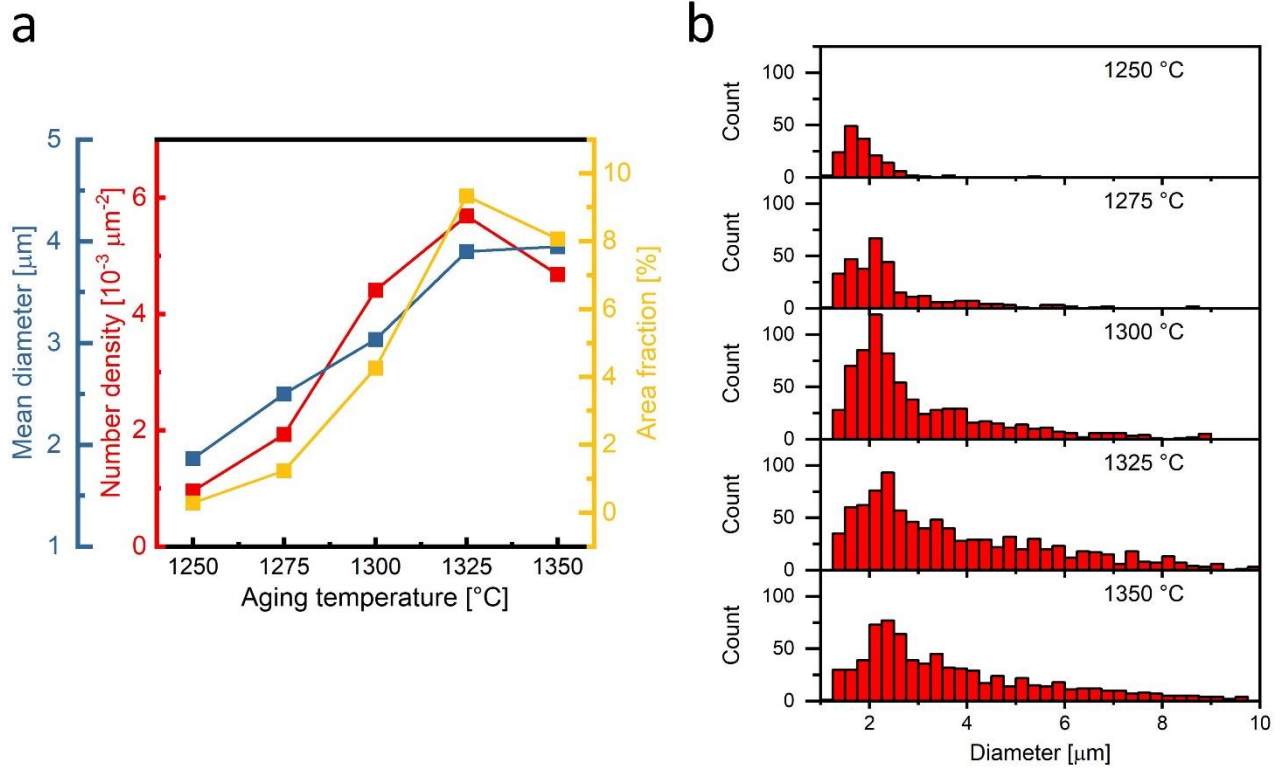


Figure S2. Quantification of precipitates in BCT20 samples treated at different aging temperatures between 1250 °C and 1350°C (one-step aging). (a) Area number density, mean diameter, and area fraction. (b) Size distribution of precipitates in the BCT20 aged at different temperatures for 8 h. The statistical data was obtained from SEM images using the back-scattered electron imaging mode. A total area of about 0.166 mm<sup>2</sup> was analyzed.

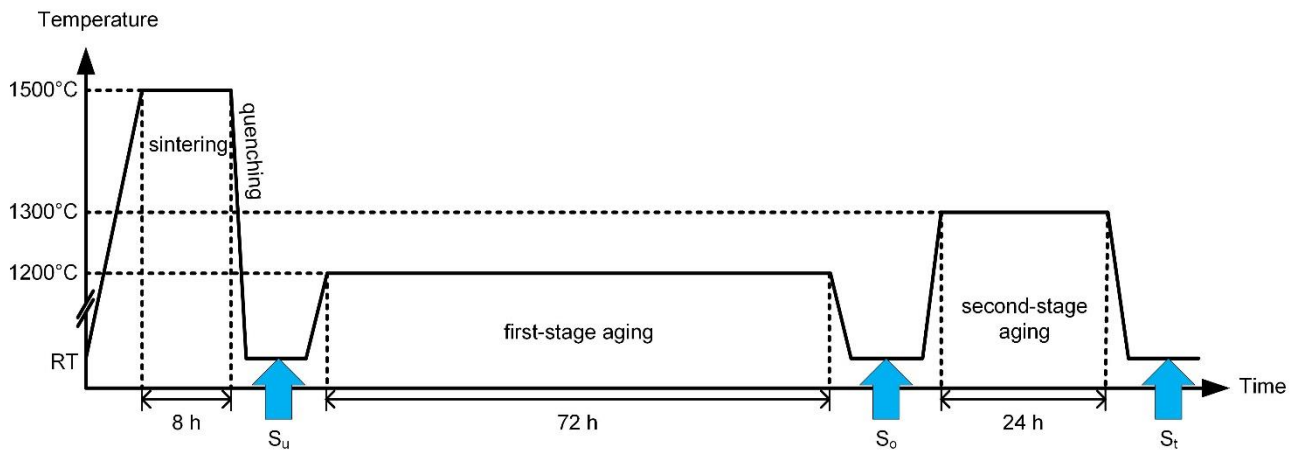


Figure S3. Temperature profile of the processing of the BCT20 samples  $S_u$ ,  $S_o$ , and  $S_t$ . The samples were obtained after the quenching process, first-stage aging, and second-stage aging, respectively.

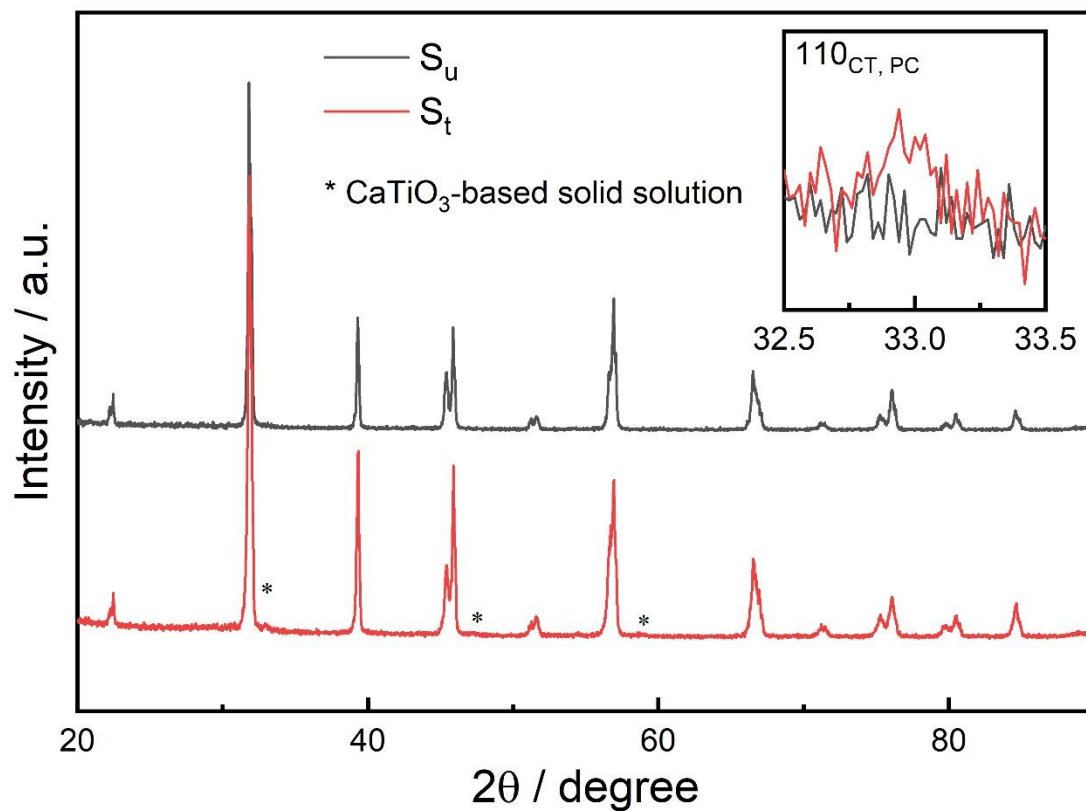


Figure S4. XRD patterns of the  $S_u$  and  $S_t$  samples. The star symbols represent the reflections from precipitates of the  $\text{CT}_{ss}$  phase in the  $S_t$  sample.

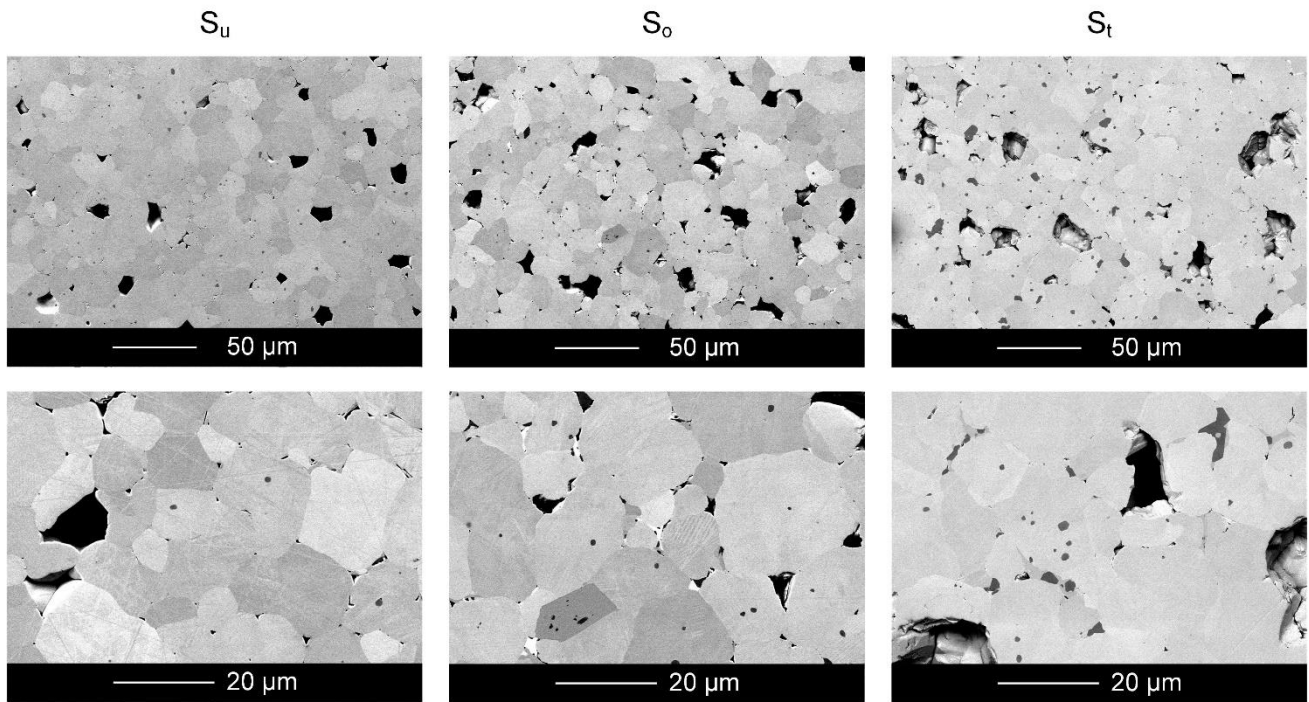


Figure S5. SEM images (back-scattered electron mode) of the polished  $S_u$ ,  $S_o$  and  $S_t$  samples with different magnifications. While a small amount of precipitates can still be observed in the  $S_u$  sample due to the limited cooling rate in air quenching, the number of intragranular precipitates increases strongly in the  $S_o$  sample. Compared to the  $S_o$  sample, the  $S_t$  sample has precipitates with larger size, and the precipitates at the grain boundaries become significant.

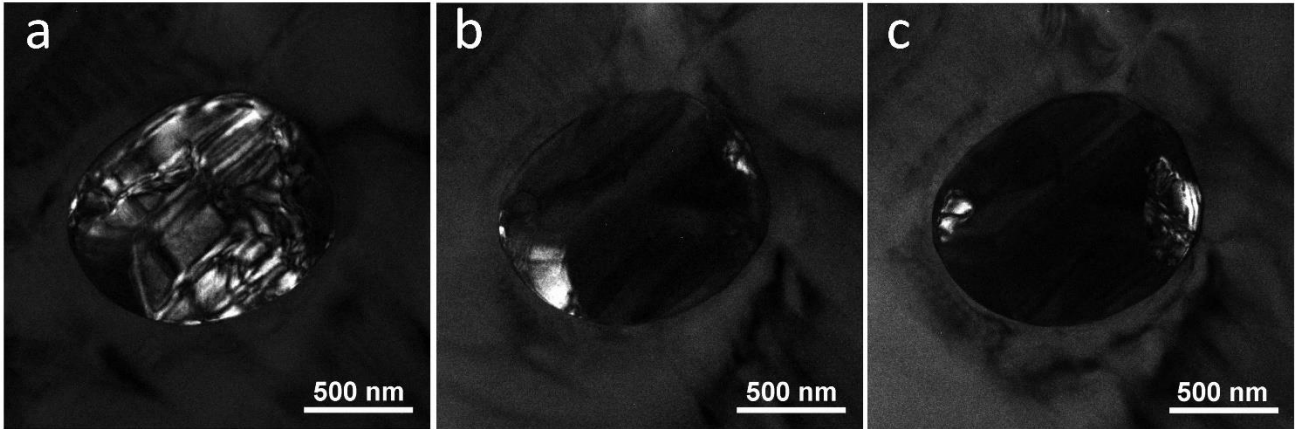


Figure S6. Dark field TEM images obtained using (a)  $\frac{1}{2}(10\bar{1})$ , (b)  $\frac{1}{2}(1\bar{1}0)$ , and (c)  $\frac{1}{2}(0\bar{1}1)$  superlattice reflections, which are circled in Figure 2d. The bright area in Figure S6a is much larger than that in Figure S6b and S6c, which is consistent with the SAED pattern in Figure 2d that, the intensity of  $\frac{1}{2}(10\bar{1})$  reflection is clearly stronger than the intensity of  $\frac{1}{2}(1\bar{1}0)$  and  $\frac{1}{2}(0\bar{1}1)$ .



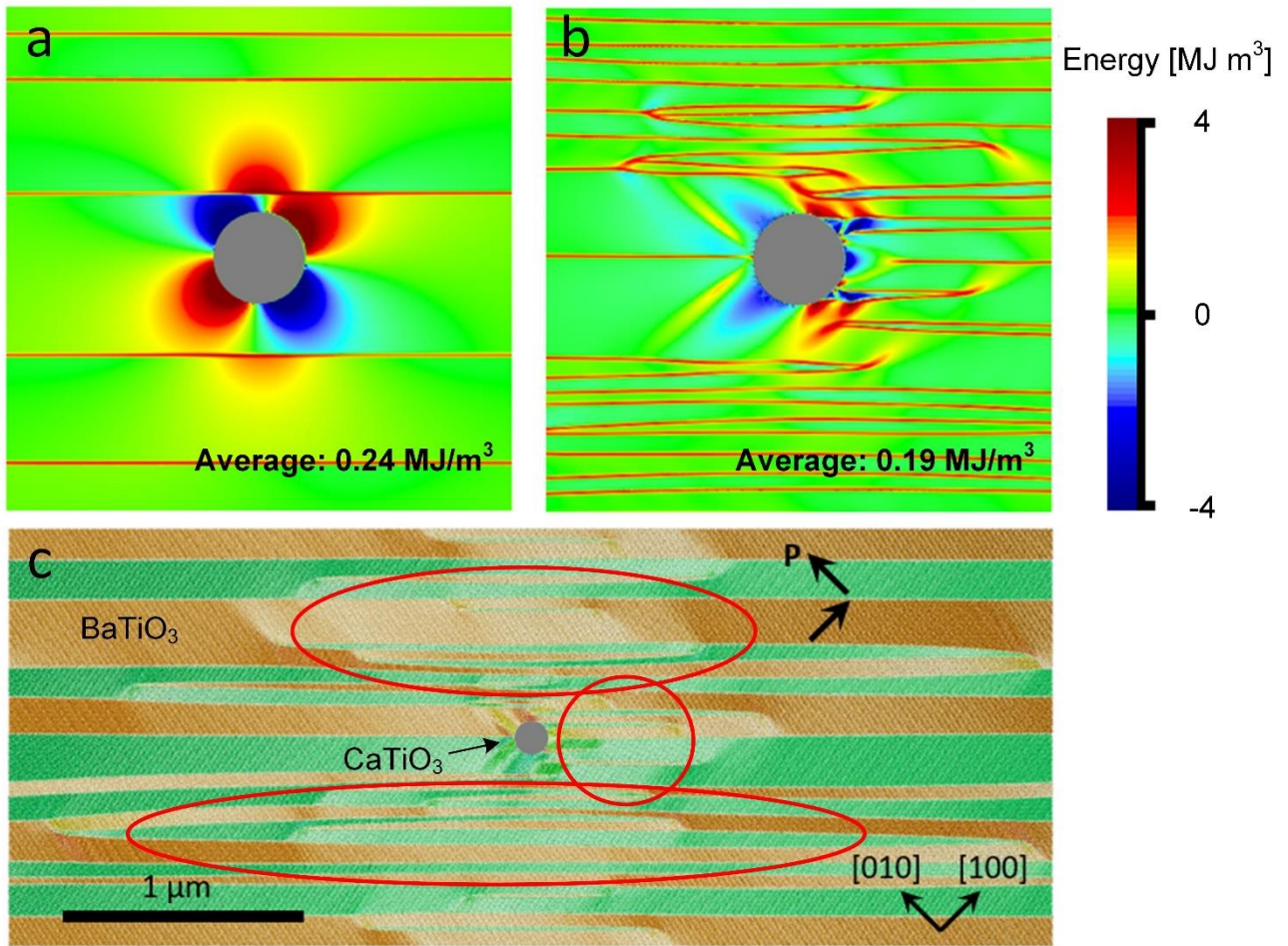


Figure S7. Calculated distributions of the electrostatic free energy density in the (a) absence and (b) presence of the fine domain structure. The electrostatic free energy density is given by  $f_{elec} = -\epsilon_0 \epsilon^b E^2 / 2 - \mathbf{E} \cdot \mathbf{P}$ , where  $\epsilon^b$  is the background dielectric constant and  $\mathbf{E}$  is the local electric field. (c) Large-area phase-field simulation of the domain configuration near a precipitate.

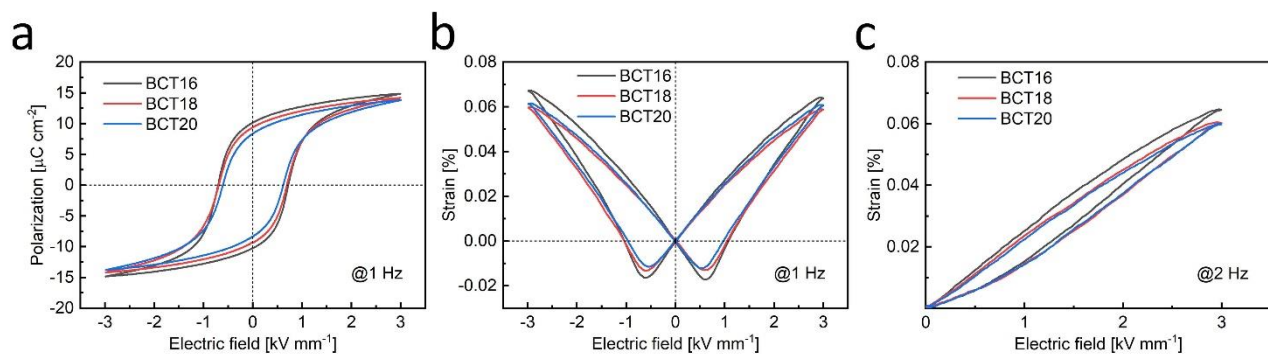


Figure S8. Bipolar (a) polarization and (b) strain hysteresis loops, and (c) unipolar strain loops of unaged BCT samples with different compositions ( $\text{CaTiO}_3$  wt.% = 0.16, 0.18, and 0.20)

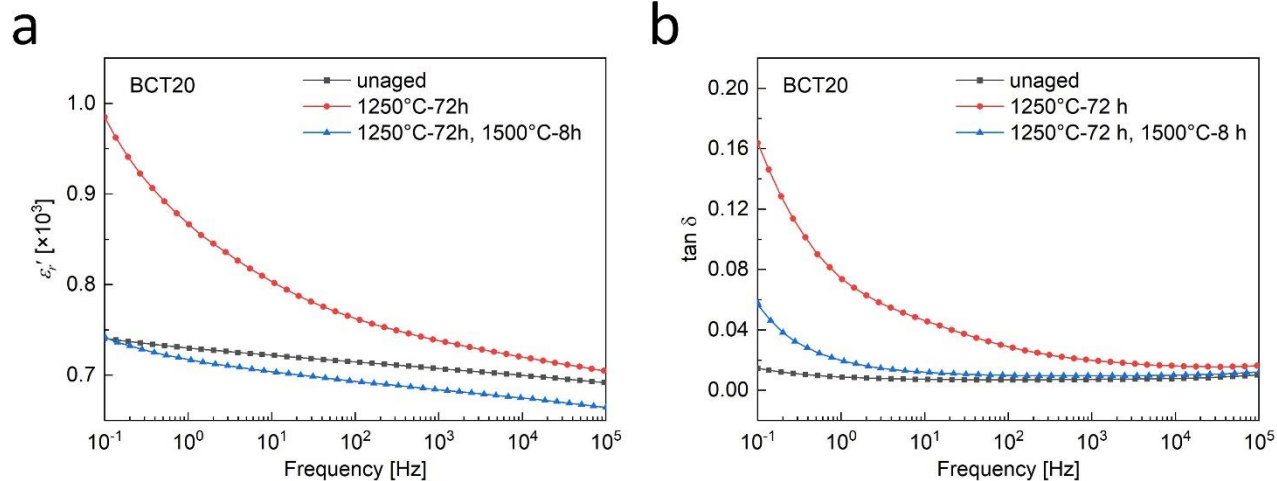


Figure S9. Real part of the permittivity and dielectric loss as a function of frequency of the BCT20 samples which are unaged, aged at 1200°C for 72 h, and aged at 1200°C for 72 h followed by a quenching from 1500°C.

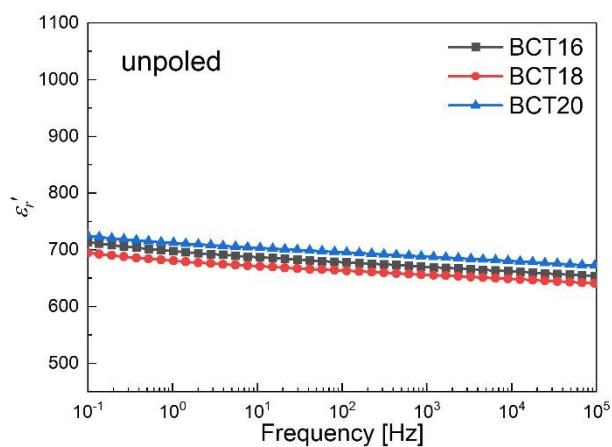


Figure S10. Permittivity of unpoled BCT samples with different Ca content as a function of frequency. The unaged BCT samples without precipitates have comparable permittivity-frequency behaviors in the Ca content range of 16 wt.% to 20 wt.%, indicating that the compositional changes in BCT (Ba/Ca ratio) have negligible influence on permittivity.

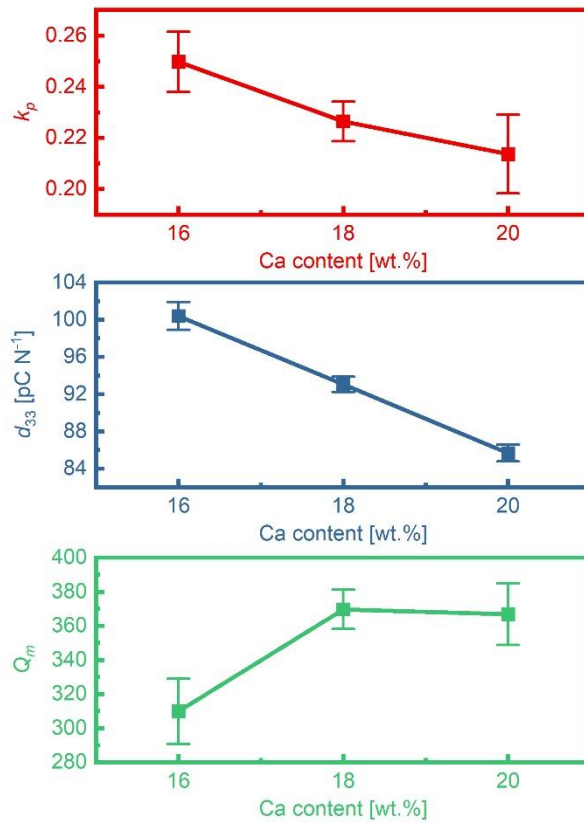


Figure S11. Planar electromechanical coupling factor  $k_p$ , longitudinal piezoelectric coefficient  $d_{33}$ , and small-signal mechanical quality factor in planar vibration mode  $Q_m$  of BCT samples with different compositions.

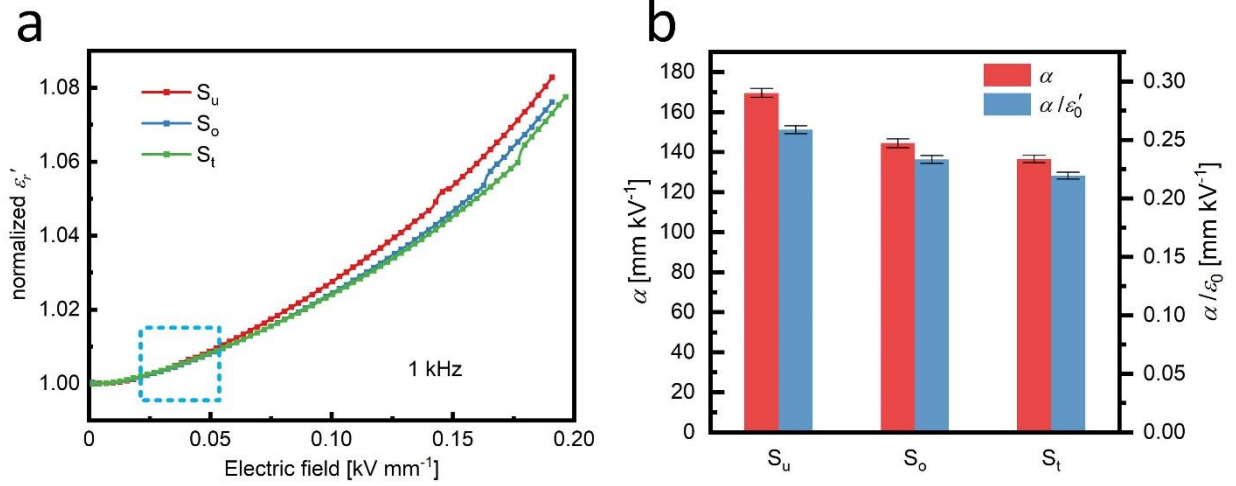


Figure S12. Rayleigh measurement results of the  $S_u$ ,  $S_o$  and  $S_t$  samples. According to the Rayleigh theory, the permittivity at subcoercive field can be expressed as:  $\epsilon'_r(E) = \epsilon'_0 + \alpha E$ , where  $\epsilon'_r(E)$  is the permittivity at a field with amplitude of  $E$ ;  $\epsilon'_0$  is the permittivity of the sample at extremely small field, where the contributing mechanisms are in principle intrinsic lattice effect and reversible domain wall motion;  $\alpha$  is the nonlinear dielectric coefficient, which describes the field-amplitude dependence of the permittivity and results from irreversible domain wall motion. (a) Normalized permittivity as a function of the field amplitude. The normalization factor is the permittivity at the smallest field, which is close to  $\epsilon'_0$ ; (b) The  $\alpha$  values (red bars) extracted from linear fitting of the  $\epsilon'_r$ - $E$  curve in the region indicated by the blue dashed square, as well as the ratio of  $\alpha$  to  $\epsilon'_0$  (blue bars).

Table S1. Coercive fields  $E_c$  of the  $S_u$ ,  $S_o$ , and  $S_t$  samples. The  $E_c$  values were extracted from the polarization hysteresis measurement with a bipolar electric field with  $|E_{max}| = 2$  kV/mm.

Samples	$S_u$	$S_o$	$S_t$
$E_c$ [kV mm <sup>-1</sup> ]	0.60	0.54	0.58